PASJ: Publ. Astron. Soc. Japan **58**, 847–860, 2006 October 25

Three-Dimensional Distribution of the ISM in the Milky Way Galaxy: II. The Molecular Gas Disk

Hiroyuki NAKANISHI
Nobeyama Radio Observatory, Minamimaki, Minamisaku, Nagano 384-1305
hnakanis@nro.nao.ac.jp
and
Yoshiaki SOFUE
Institute of Astronomy, The University of Tokyo, 2-21-1 Osawa, Mitaka, Tokyo 181-0015

(Received 2006 February 14; accepted 2006 August 3)

Abstract

We created a three-dimensional distribution map of molecular gas throughout the Milky Way galaxy using the latest ^{12}CO ($J = 1$–0) survey data cube and the rotation curve based on the kinematic distance. The radial distribution of the molecular gas shows a central peak and a second peak around 0.5 R_0 (R_0: the solar Galactocentric distance). The thickness of the molecular disk slightly increases from 48 pc to 160 pc with the Galactocentric distance within a radius range of 0–11 kpc. We were able to trace the Outer, the Perseus, the Sagittarius–Carina, the Scutum–Crux, and the Norma arms as logarithmic spiral arms with pitch angles of 11°–15°. Considering that the pitch angles of the spiral arms are within this range, the Norma and the Outer arms seem to be identified as the same spiral arm. We could also trace a midplane displacement, whose amplitude is nearly constant inside a 10 kpc radius and increases beyond this radius. The ridges of the midplane displacement form the leading spiral arms.

Key words: Galaxy: disk — Galaxy: kinematics and dynamics — Galaxy: structure — ISM: kinematics and dynamics — radio lines: ISM

1. Introduction

The global three-dimensional (3D) structure of the Milky Way galaxy is one of the essential informations to study the Galactic objects in detail. In Paper I (Nakanishi, Sofue 2003), we analyzed the latest 21-cm line survey data, and presented a 3D distribution map of H I gas in the Milky Way galaxy. In this paper, we treat the molecular gas distribution as Part II of this series.

A survey in the ^{12}CO (J = 1–0) line is a good tool for tracing the interstellar matter (ISM) in the inner disk of the Milky Way galaxy (inside the solar orbit), while the H I data is advantageous for a study of the ISM in the outer disk (outside the solar orbit). One of the most famous CO line surveys is the Columbia CO survey, whose earlier survey was carried out with the 1.2-m telescopes in New York City, USA, and Cerro Tololo, Chile (Dame et al. 1987; Bronfman et al. 1988, 1989). This survey covered the entire Milky Way with a grid spacing of 0.°5. Another higher resolution survey is the Massachusetts–Stonybrook Galactic plane CO survey, which was made using the 14-m telescope of the Five College Radio Astronomy Observatory (FCRAO) (Sanders et al. 1986). The covered ranges of the galactic longitude and latitude were from $l = 8°$ to 90° and from $b = -1.°05$ to $+1.°05$ in the first quadrant, respectively. The grid spacing was $3' \times 3'$ or $6' \times 6'$. These large CO surveys were indispensable for exploring the molecular gas distribution in the Milky Way galaxy. There have been several studies of the Galactic structure using these data.

Dame et al. (1986) and Myers et al. (1986) showed face-on views of the first Galactic quadrant while examining the positions of the largest individual molecular complexes identified in the Columbia CO survey of the first Galactic quadrant (Cohen et al. 1986). They found clear evidence for the Sagittarius spiral arm. Cohen et al. (1985) and Grabelsky et al. (1987, 1988) showed the distribution of giant molecular clouds in the fourth quadrant, and they clearly delineated the Carina arm. Clemens, Sanders, and Scoville (1988) presented the molecular gas distribution in the first quadrant of the inner disk of the Milky Way galaxy using the Massachusetts–Stoneybrook CO survey, found a ring-like structure at a radius of 0.5 R_0 (R_0: the Galactocentric distance of the Sun), and traced the Sagittarius and Perseus arms. The distance of the molecular gas was determined by the kinematic distance using a rotation curve. The near–far problem in the inner Galaxy was overcome by introducing a vertical model of the molecular gas distribution. Solomon and Rivolo (1989) showed a face-on view of the Milky Way galaxy by examining individual giant molecular clouds identified in the Massachusetts–Stoneybrook CO survey.

Hunter et al. (1997) presented the molecular gas distributions in the entire Galactic disk of the Milky Way galaxy using the Columbia survey (Dame et al. 1987) for modeling the diffuse gamma-ray emission. The distance of the molecular gas was determined by the kinematic distance. Although there is a near–far problem in the inner disk, they divided the gas density equally at near and far points for $b = 0°$.

Sawada et al. (2004) determined the molecular gas distribution at the Galactic center by considering the absorption of the OH line to determine the line-of-sight distance of the molecular gas, using the CO data cube of Bitran et al. (1997). They found that the molecular gas is elongated in the line-of-sight direction against the Sun, and that this feature is associated with

a central galactic bar.

Thus, there have been several studies on the molecular gas distribution. However, there has been no three-dimensional gas density map of the whole Galaxy. Dame, Hartmann, and Thaddeus (2001) published a new compilation of the Columbia ^{12}CO (J = 1–0) survey of the whole Milky Way galaxy. The sampling and the sensitivity of this survey were much improved over that of the old Columbia survey. This is a great tool for investigating the molecular gas distribution throughout the entire Milky Way galaxy. In this paper, we show a molecular gas distribution in the Milky Way galaxy using the Columbia ^{12}CO (J = 1–0) survey data and the latest rotation curve.

2. Data

We used the latest compilation of ^{12}CO (J = 1–0) survey data (Dame et al. 2001), which were obtained with the 1.2-m telescopes in New York City, USA, and Cerro Tololo, Chile. The half-power beam width (HPBW) was 8′.4, which corresponded to 2.4 pc at the heliocentric distance of 1 kpc. The data consisted of ^{12}CO (J = 1–0) line spectra over the entire Milky Way. We used data of surveys named 2, 8, 18, 31, 33, and 36. The grid spacing of these data was 0°.125–0°.25. The total radial velocity (V_r) coverage was 332 km s^{-1} and the velocity resolution was 1.3 km s^{-1}. The rms noise level per channel was 0.12–0.43 K. We used spectra within a Galactic latitude range of $|b| \leq 1.5°$.

The rotation curve, which we used to transform the radial velocity of the CO gas into the distance, was the same as we used in Paper I. The inner and outer rotation curves are taken from Clemens (1985) and Dehnen and Binney (1998), respectively. The Galactic constants R_0 = 8.0 kpc (the Galactocentric distance of the Sun) and V_0 = 217 km s^{-1} (the solar rotational velocity) are adopted.

3. Method

3.1. Binding the Data

3.1.1. Inner Galaxy

For the inner Galaxy, we averaged the CO data over five channels ($\geq$ 6.5 km s^{-1} velocity width) for each spectrum in order to eliminate the cloud-cloud motion of 3–3.9 km s^{-1} (Clemens 1985; Alvarez et al. 1990) and to obtain a higher signal-to-noise ratio (S/N ratio).

The molecular gas is distributed in a more clumpy form than the H I gas. Since we intend to develop our understanding of the global structure of the Milky Way galaxy, we must smooth the CO emission on a larger scale in order to eliminate such clumpy features and to model the vertical structure of the molecular gas disk. Since the typical scale of the random motion of the molecular clouds is 0.015 R_0 kpc (Clemens 1985), we averaged the data over a 240 pc width when the line-of-sight length corresponding to 6.5 km s^{-1} velocity width was smaller than 240 pc. Thus, the CO data were averaged over $\geq$ 6.5 km s^{-1} velocity width and $\geq$ 240 pc width.

In addition, we averaged the data in the longitudinal direction to eliminate the clumpy features of CO clouds and to obtain a much higher S/N ratio. For the first ($0° \leq l \leq 90°$) and fourth ($270° \leq l \leq 360°$) quadrants, we bound the data, so that the longitudinal width at the tangential point would be equal to 240 pc width.

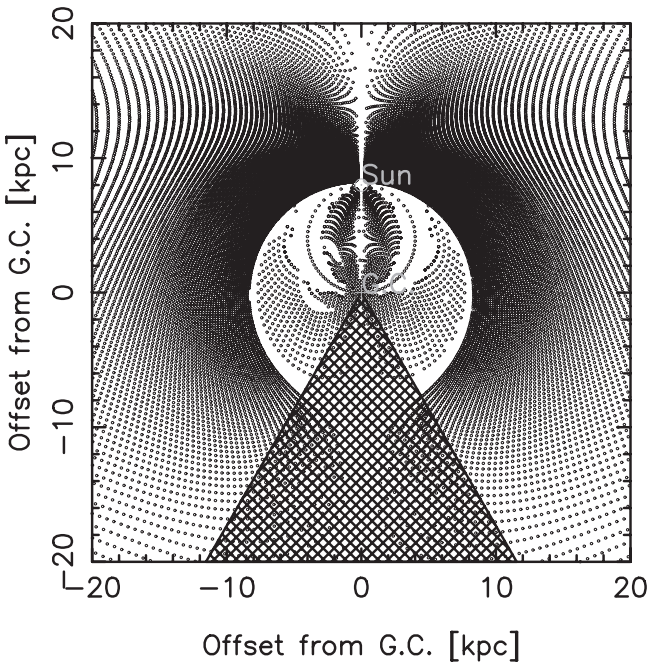

Fig. 1. Grid points where gas densities were calculated. The hashed area denotes a region where there are too few points to make a density map.

Thus the CO data were averaged over $\geq$ 240 pc in the line-of-sight direction and longitudinal direction, except for the inner region of the tangential radius, where the data were averaged over $\geq$ 240 pc width only in the line-of-sight direction. The data were not averaged in the latitudinal direction at all.

3.1.2. Outer Galaxy

For the outer Galaxy, we averaged the data in the longitudinal direction so that the longitudinal separation became 0°.5, which is nearly the same as the H I data. Moreover, we averaged the CO data over two channels ($\geq$ 2.6 km s^{-1} velocity width), which is also the same as the H I data.

Figure 1 shows the points where the molecular gas densities were calculated.

3.2. Molecular Gas Distribution in the Outer Galaxy

In the present work, we chose a Cartesian coordinate whose x-axis coincided with the line crossing the Sun and the Galactic center, and whose origin coincided with the Galactic center. The z-axis was chosen so that it would be parallel to the rotational axis. The Sun was located at $(-8\,\mathrm{kpc}, 0, 0)$. We also chose cylindrical coordinates (R, θ, z) so that the angle $\theta = 180°$ coincided with the direction toward the Sun and the angle $\theta = 90°$ was parallel to $l = 90°$.

The distance of the molecular gas was determined by the kinematic distance here as in Paper I. The distance of molecular gas in the outer disk ($R > R_0$) was uniquely determined, and we then obtained the molecular gas distribution in the outer disk using the equation

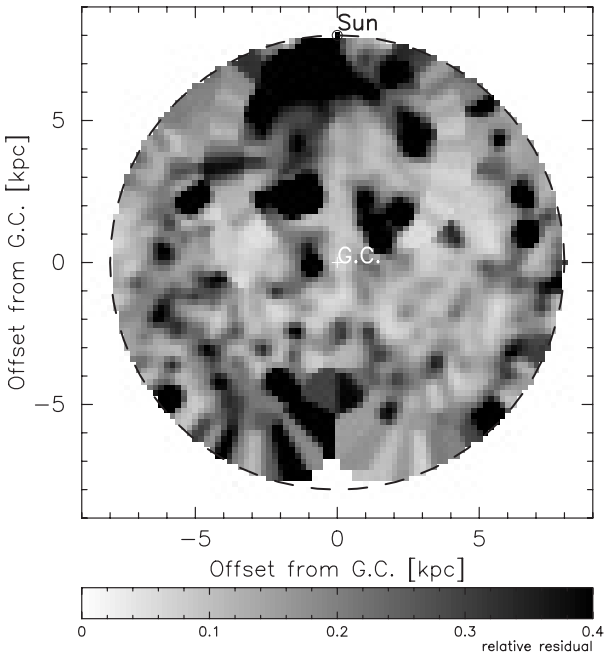

Fig. 2. Residual map. We here define the "relative residual" to be a fraction of the standard deviation of residuals between fitted model curves and observation data relative to the peaks of the observation data.

$$n_{\mathrm{H_2}} = X T_{\mathrm{b}} \frac{\Delta V_{\mathrm{r}}}{\Delta r}, \tag{1}$$

where $n_{\mathrm{H_2}}$ denotes the volume number density of the molecular hydrogen, $\mathrm{H_2}$, X the CO-to-$\mathrm{H_2}$ conversion factor, and r the heliocentric distance. We adopted two kinds of conversion factor: (1) a constant conversion factor of $X = 1.8 \times 10^{20}$ ($\mathrm{H_2\,cm^{-2}\,K^{-1}/km\,s^{-1}}$) (Dame et al. 2001) and (2) a varying conversion factor with the Galactocentric distance (Arimoto et al. 1996). Arimoto, Sofue, and Tsujimoto (1996) calculated X using the data in Solomon et al. (1987).

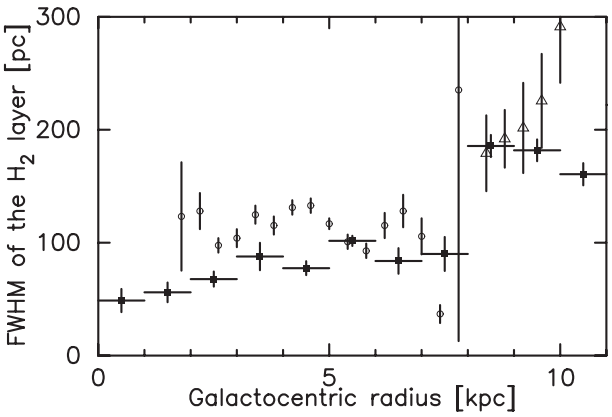

Fig. 3. FWHM of the $\mathrm{H_2}$ gas layer versus the Galactocentric radius. The filled squares, open circles, and open triangles denote the data from the present study, Bronfman et al. (1988), and Grabelsky et al. (1987), respectively.

Since the conversion factor can be approximately expressed by an exponential function of the Galactocentric radius, we fitted an exponential function to the resultant radial profile and obtained the following equation:

$$X\ [\mathrm{H_2\,cm^{-2}\,K^{-1}/km\,s^{-1}}] = 1.4 \times 10^{20} \exp(R/11\,\mathrm{kpc}). \tag{2}$$

3.3. *Molecular Gas Distribution in the Inner Galaxy*

There is, on the other hand, a near–far ambiguity in the inner disk ($R < R_0$); i.e., there are two heliocentric distances satisfying the same radial velocity. Therefore, we could not determine the $\mathrm{H_2}$ distribution in the inner Galaxy in the same way as in the outer Galaxy. In order to divide the molecular distributions at the near and far points, we introduced a vertical

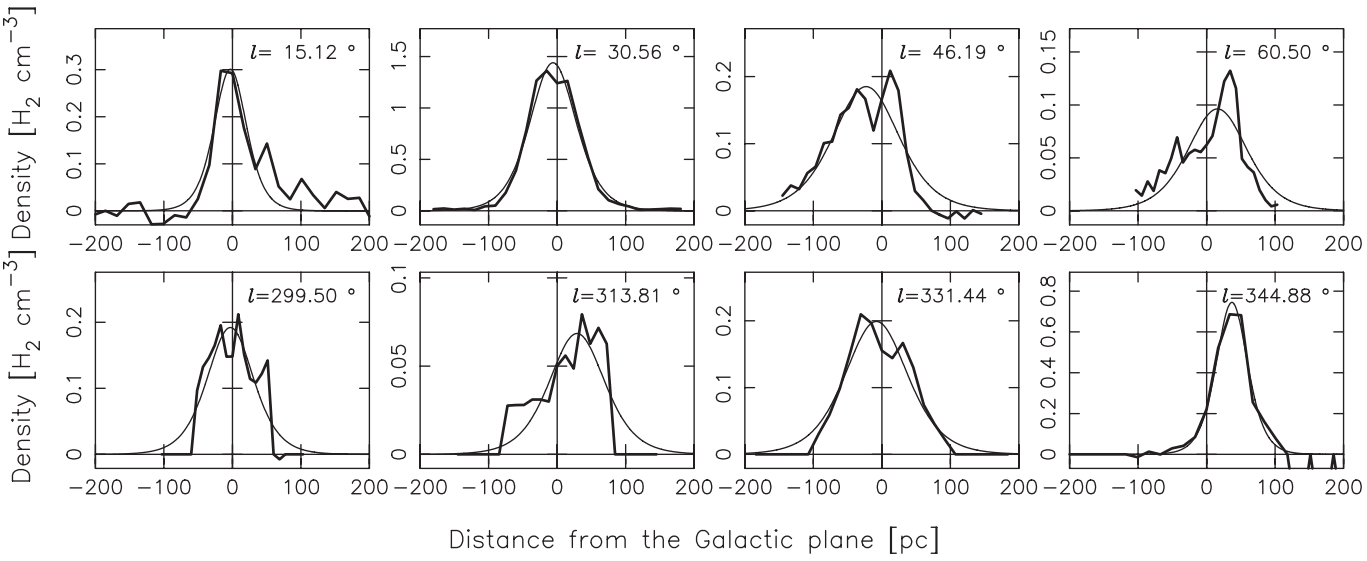

Fig. 4. Vertical distributions of the molecular gas. The horizontal and vertical axes denote the height from the Galactic plane ($b = 0°$) and $\mathrm{H_2}$ density, respectively. The thick and thin lines indicate observation data and a model curve, respectively.

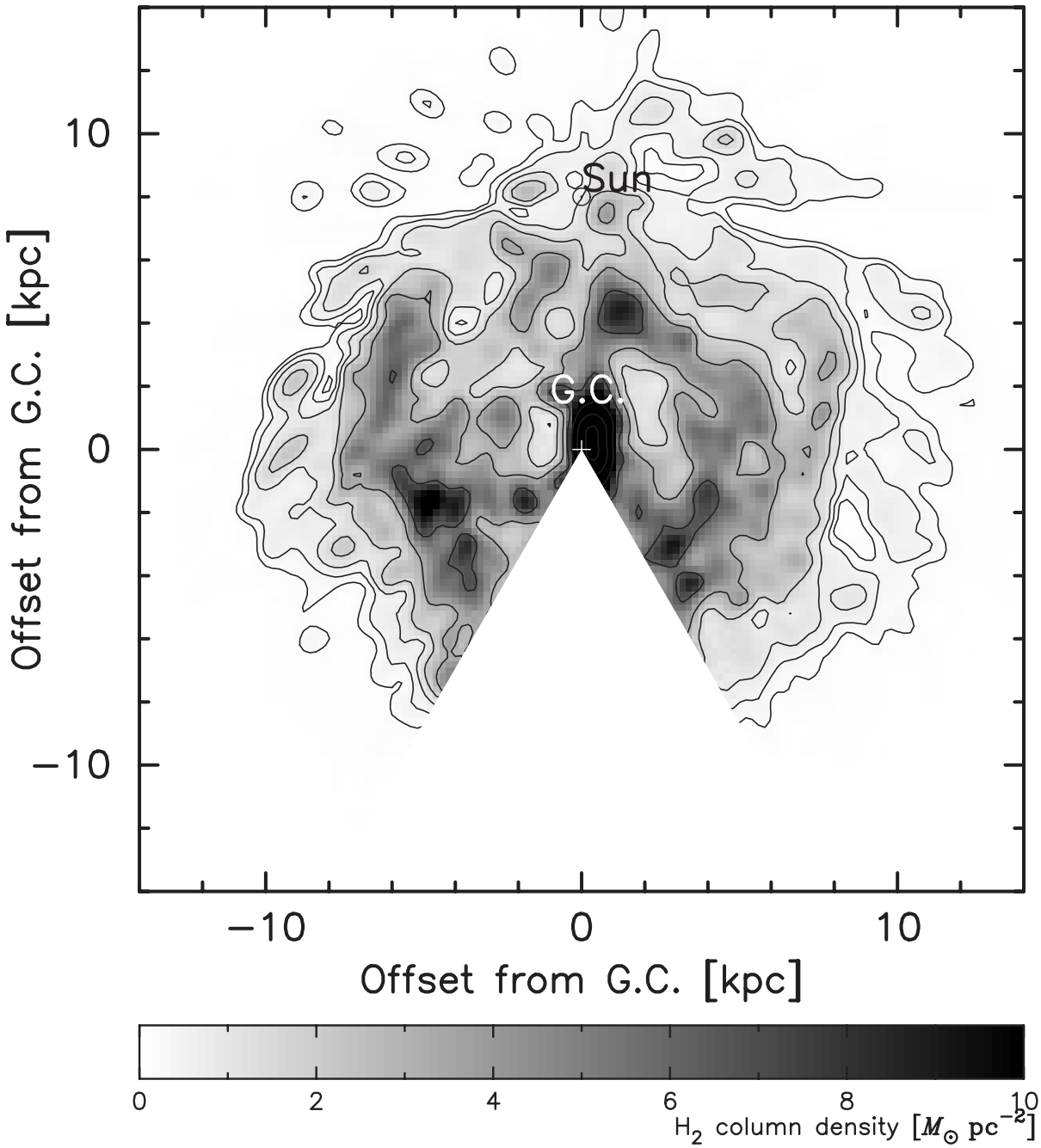

Fig. 5. Face-on molecular hydrogen map obtained by adopting the constant conversion factor of $X = 1.8 \times 10^{20}$ (Dame et al. 2001). The contour levels are 0.2, 0.4, 0.8, 1.6, 3.2, 6.4, and 12.8 $M_\odot\,\mathrm{pc}^{-2}$.

structure of the Galactic disk. Following Spitzer (1942), we assumed that the vertical distribution of the molecular gas is expressed with

$$n(z) = n_0\,\mathrm{sech}^2(\xi), \tag{3}$$

$$\xi = \log\left[(1+\sqrt{2})\frac{z-z_0}{z_{1/2}}\right], \tag{4}$$

where z and $z_{1/2}$ denote the height from the Galactic plane ($b = 0^\circ$) and the scale-height, respectively. At $z = z_{1/2}$ the density, n, has a half value of the maximum at the midplane. The subscript 0 means values at the midplane. The scale-height was determined at the tangential points in the inner Galaxy, which is described in the next subsection.

Assuming that the vertical distribution of the H_2 gas follows equation (3), the H_2 column density, $N_{H_2}(b)$, is represented as a function of the Galactic latitude, b, using four parameters: n_{H_21}, n_{H_22}, z_{0_1}, and z_{0_2}. That is,

$$N_{H_2}(b) = n_{H_21}\,\mathrm{sech}^2(\xi_1)\frac{\Delta r_1}{\cos b} + n_{H_22}\,\mathrm{sech}^2(\xi_2)\frac{\Delta r_2}{\cos b}, \tag{5}$$

where

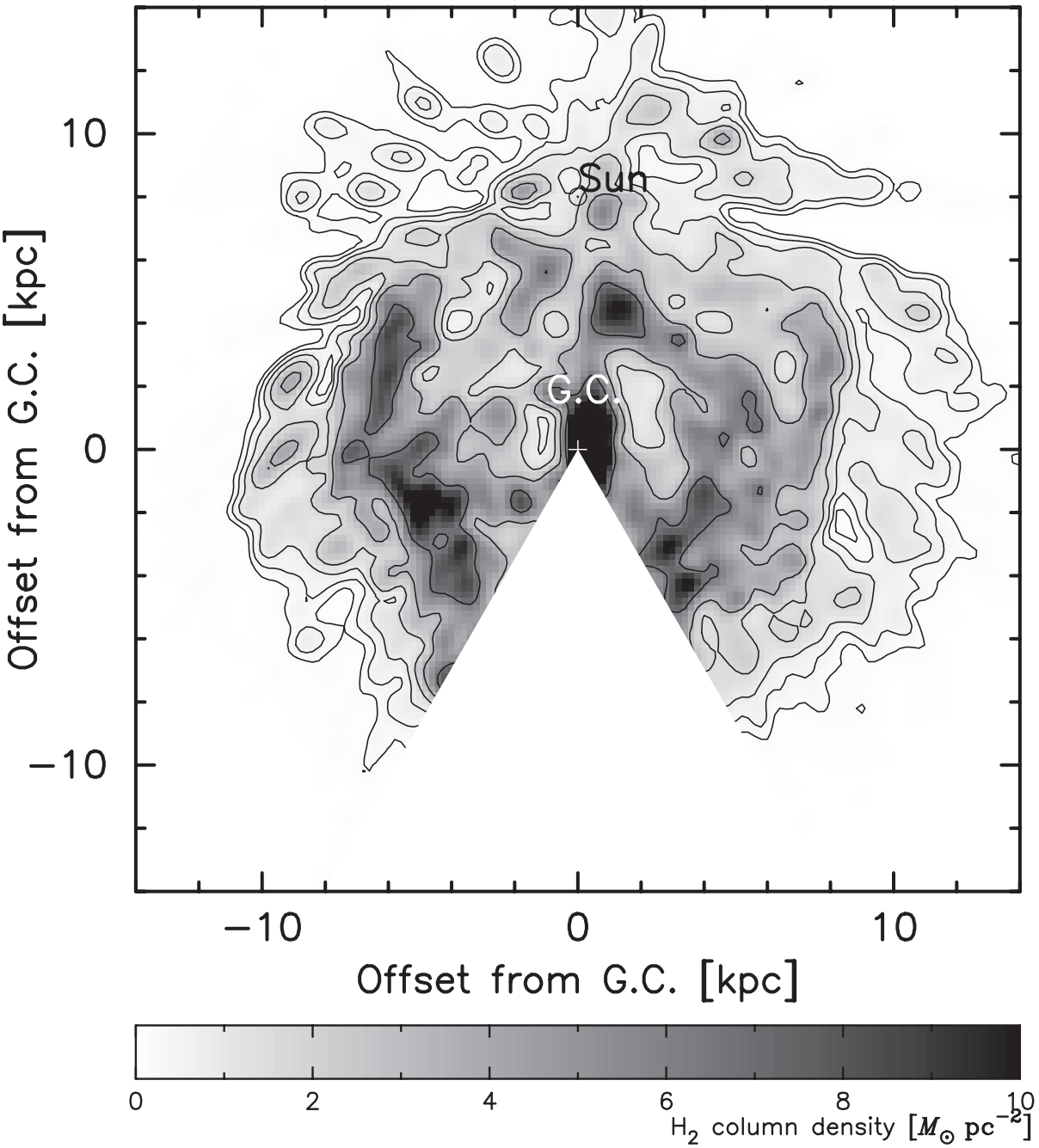

Fig. 6. Face-on molecular hydrogen map obtained by adopting the conversion factor X taken from Arimoto, Sofue, and Tsujimoto (1996), where X increases exponentially with the Galactocentric distance. The contour levels are the same as those of figure 5.

$$\xi_1 = \log\left[(1+\sqrt{2})\frac{r_1 \tan b - z_{0_1}}{z_{1/2}}\right], \tag{6}$$

$$\xi_2 = \log\left[(1+\sqrt{2})\frac{r_2 \tan b - z_{0_2}}{z_{1/2}}\right]. \tag{7}$$

For each point shown in figure 1, we sought a parameter set consisting of $n_{\mathrm{H}_2 1}$, $n_{\mathrm{H}_2 2}$, z_{0_1}, and z_{0_2}, which gives the smallest residual in subtracting the model distribution from the observation. The fitting resolution of the four parameters is $0.01\,\mathrm{H_2\,cm^{-3}}$ for $n_{\mathrm{H}_2 1}$ and $n_{\mathrm{H}_2 2}$ and 1 pc for z_{0_1} and z_{0_2}, respectively. We restricted z_{0_1} and z_{0_2} to within a range of -250 pc to $+250$ pc. The grid spacing was $0.^{\circ}125$, which corresponds < 17 pc at tangential points, at most points in the inner Galaxy. Since there were enough points (more than three points) to resolve near vertical distribution, it was possible to divide the total CO emission into near and far emissions. We thus obtained parameter sets of $n_{\mathrm{H}_2 1}$, $n_{\mathrm{H}_2 2}$, z_{0_1}, and z_{0_2} for discrete points in the inner Galaxy.

To show how well the fitting method works, we present a residual map (in figure 2). In order to make this map, we first measured the standard deviation of residuals between a fitted

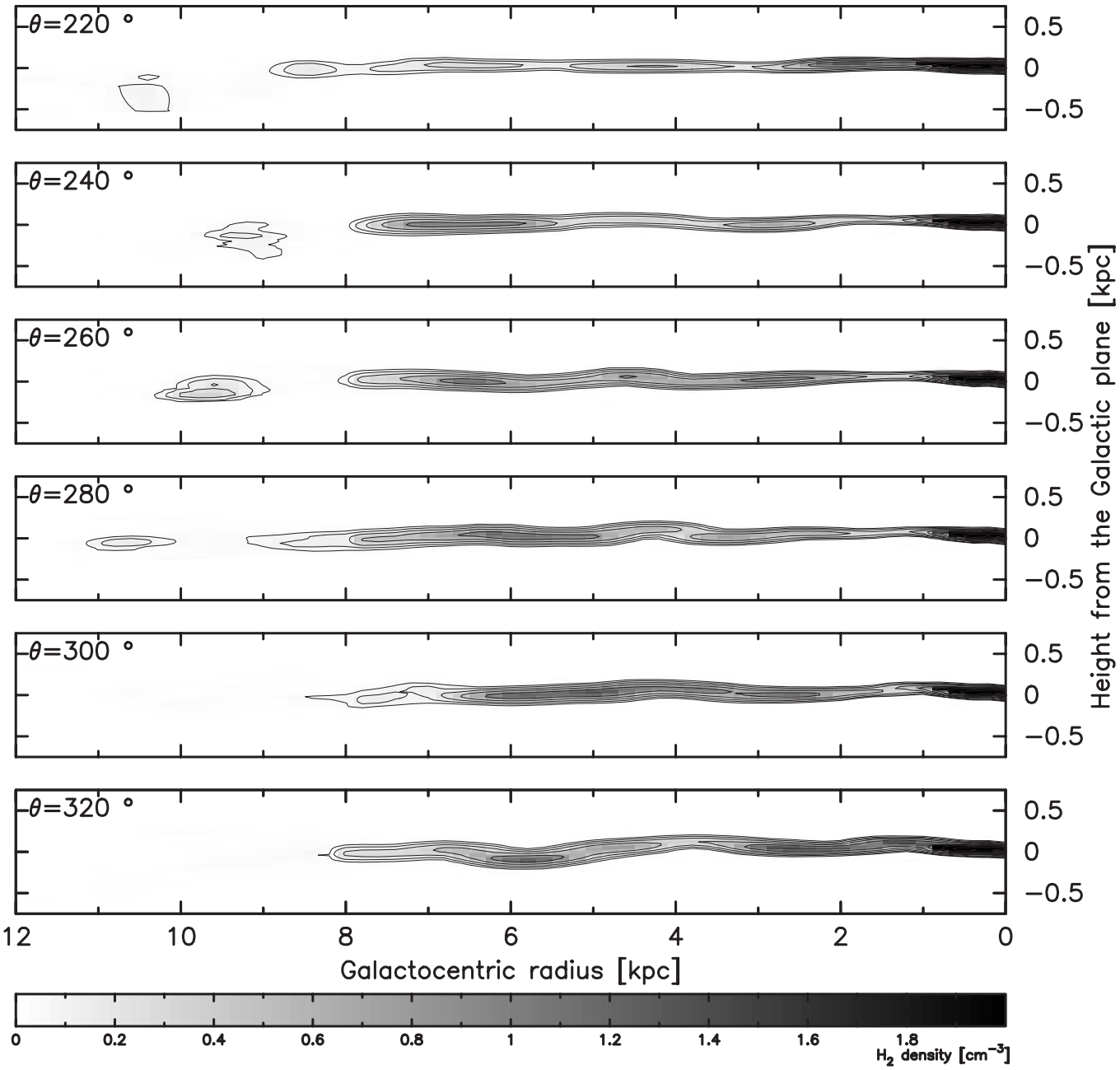

Fig. 7. Longitudinal section maps. Each map shows the H_2 volume densities in a sheet through the Galactic center perpendicular to the Galactic plane. Individual panel shows sections through $\theta = 220°$, $\theta = 240°$, $\theta = 260°$, $\theta = 280°$, $\theta = 300°$, and $\theta = 320°$. The contours are drawn at levels of 0.05, 0.1, 0.2, 0.4, 0.8, 1.6, and 3.2 H_2 density [cm^{-3}].

model curve and the observed data. We then calculated the relative residuals, which is a fraction of the standard deviation relative to the peak of the observational data. This residual map shows that the relative residual is less than 20–30% in most of the region, and that the fitting method does not work well near the Sun.

3.4. Scale-Height

Tangential points that satisfy $R = R_0 \sin l$ present no near–far problem in the inner Galaxy. Hence, the vertical structure at the tangential point can be determined uniquely.

Gas having a velocity range $|V_{r,max} - \sigma| < |V_r| < \infty$ is located at the tangential points, where V_r, $V_{r,max}$, and σ are the radial velocity, maximum radial velocity, and random velocity, respectively. The random velocity was taken to be $5\,km\,s^{-1}$ (Clemens 1985). We thus obtained vertical distributions, and fitted a model distribution, $\rho(z) = \rho_0\,\mathrm{sech}^2(\xi)$, to determine a scale-height of $z_{1/2}$. Figure 3 shows the full width at half maximum (FWHM) ($2z_{1/2}$) versus the Galactocentric radius, which is the mean value in a 1 kpc bin. For comparison, figure 3 also shows the FWHM of the molecular disk calculated by Bronfman et al. (1988) and Grabelsky et al. (1987),

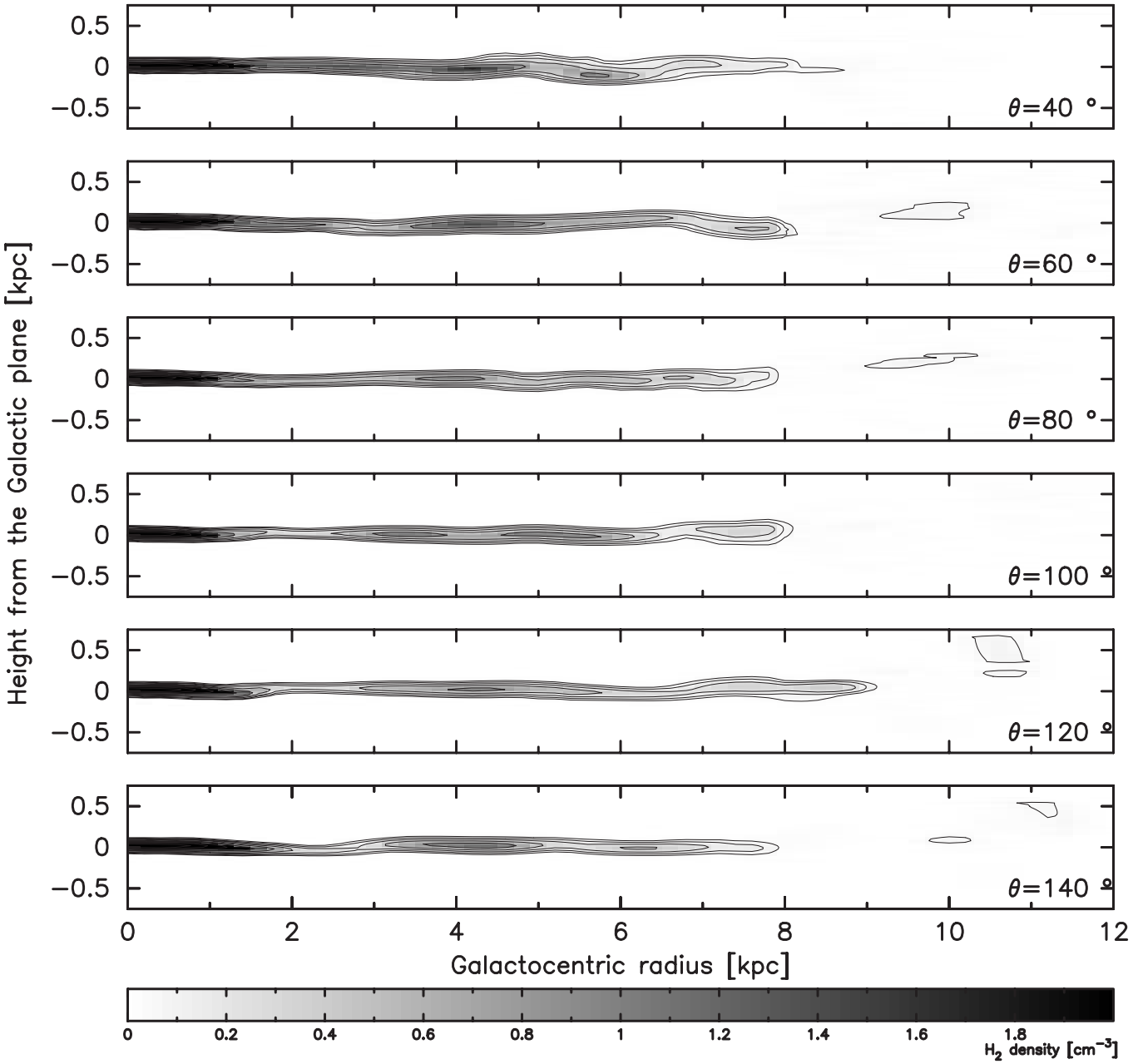

Fig. 8. Longitudinal section maps. Each map shows the H_2 volume densities in a sheet through the Galactic center perpendicular to the Galactic plane. Individual panel shows sections through $\theta = 40°$, $\theta = 60°$, $\theta = 80°$, $\theta = 100°$, $\theta = 120°$, and $\theta = 140°$. The contours are drawn at levels of 0.05, 0.1, 0.2, 0.4, 0.8, 1.6, and 3.2 H_2 density [cm^{-3}].

who used the same data as we used. We adopted the Galactic constant R_0 of 8 kpc, although Bronfman et al. (1988) and Grabelsky et al. (1987) used R_0 of 10 kpc. Therefore, the radius and FWHM were reduced by a factor of 8/10. The filled squares, open circles, and open triangles denote the data from this study, Bronfman et al. (1988), and Grabelsky et al. (1987), respectively. Our result is almost consistent with those of Bronfman et al. (1988) and Grabelsky et al. (1987).

Figure 4 shows a comparison of a model and observations. The vertical distributions of molecular gas can be approximately reproduced by equation (3).

3.5. Construction of Three-Dimensional Map

We thus obtained parameter sets of the molecular distribution at each point of figure 1.

First, the parameter sets obtained for the discrete points in the inner Galaxy were averaged with a Gaussian function whose FWHM was 0.48 kpc, in order to eliminate data with bad fitting results. Then we calculated the H_2 distribution in the inner Galaxy using the averaged parameter sets. The H_2 gas densities obtained at the discrete points in the outer Galaxy were transformed into continuous distribution by interpolating

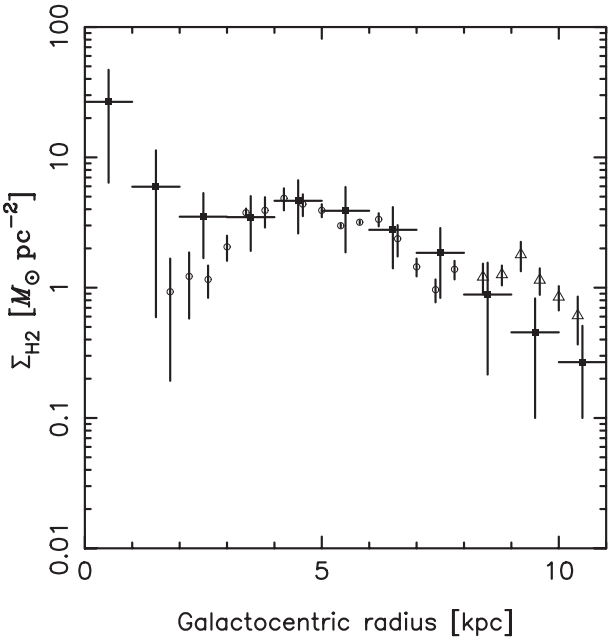

Fig. 9. Radial profiles of the H_2 gas surface density. The vertical axis is a logarithmic scale. The filled squares, open circles, and open triangles denote the data taken from the present study, Bronfman et al. (1988), and Grabelsky et al. (1987), respectively.

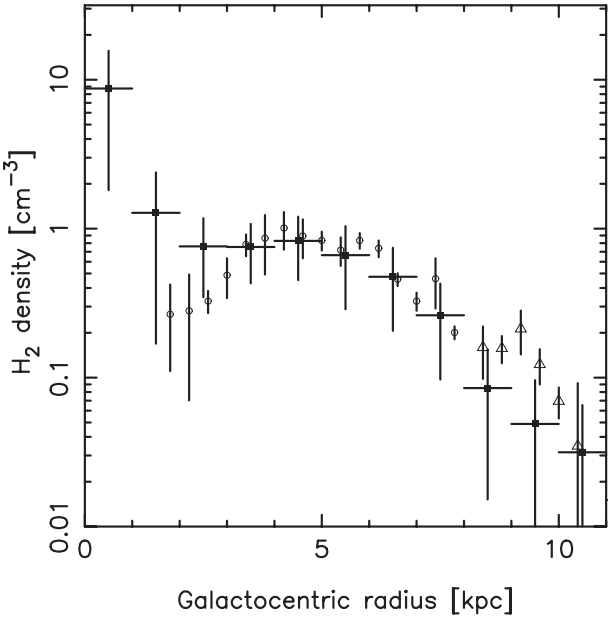

Fig. 10. Radial profiles of the H_2 gas density at the midplane. The vertical axis is a logarithmic scale. The filled squares, open circles, and open triangles denote the data taken from the present study, Bronfman et al. (1988), and Grabelsky et al. (1987), respectively.

with the same Gaussian function. The averaging length for the z-direction was fixed at 35 pc, which corresponds to a grid spacing of 0.°25 at a heliocentric distance of 16 kpc. Finally, we combined the H_2 distributions in the inner and the outer Galaxy to obtain a CO distribution cube. In this work, the grid spacing of the cube was fixed at 200 pc for the x and y directions and at 20 pc for the z direction, and the size of the resultant cube is 40 kpc $\times$ 40 kpc $\times$ 2 kpc in x, y, and z directions, respectively.

Since the number of points where the molecular gas densities were calculated (figure 1) in the azimuthal range $|\theta| < 30°$ was too few to make a map, we do not show this region.

4. Results

4.1. A Face-on Map

Figure 5 shows a face-on map of the molecular H_2 gas in the Milky Way galaxy.

Figure 6 shows a face-on map of the molecular gas when the conversion factor was calculated with equation (2). In this map, the molecular gas distribution in the outer region is slightly enhanced. However, there is no large difference between these two maps. Hence, our discussions below about the structure of the molecular gas distribution are based on the H_2 map obtained by adopting a constant conversion factor for the sake of simplicity.

Table 1. Radial variations of parameters of the molecular disk.

Radius (kpc)	Surface density ($M_\odot$ pc^{-2})	Midplane density (cm^{-3})	FWHM (pc)
0–1	26.7 ± 20.3	8.73 ± 6.91	48 ± 20
1–2	6.0 ± 5.4	1.28 ± 1.11	56 ± 18
2–3	3.5 ± 1.8	0.76 ± 0.42	68 ± 14
3–4	3.5 ± 1.6	0.75 ± 0.32	88 ± 24
4–5	4.6 ± 2.0	0.83 ± 0.38	78 ± 12
5–6	3.9 ± 2.0	0.66 ± 0.38	102 ± 10
6–7	2.8 ± 1.4	0.48 ± 0.27	84 ± 22
7–8	1.9 ± 1.0	0.26 ± 0.17	90 ± 30
8–9	0.9 ± 0.7	0.09 ± 0.07	186 ± 20
9–10	0.5 ± 0.4	0.05 ± 0.05	182 ± 20
10–11	0.3 ± 0.2	0.03 ± 0.03	160 ± 20

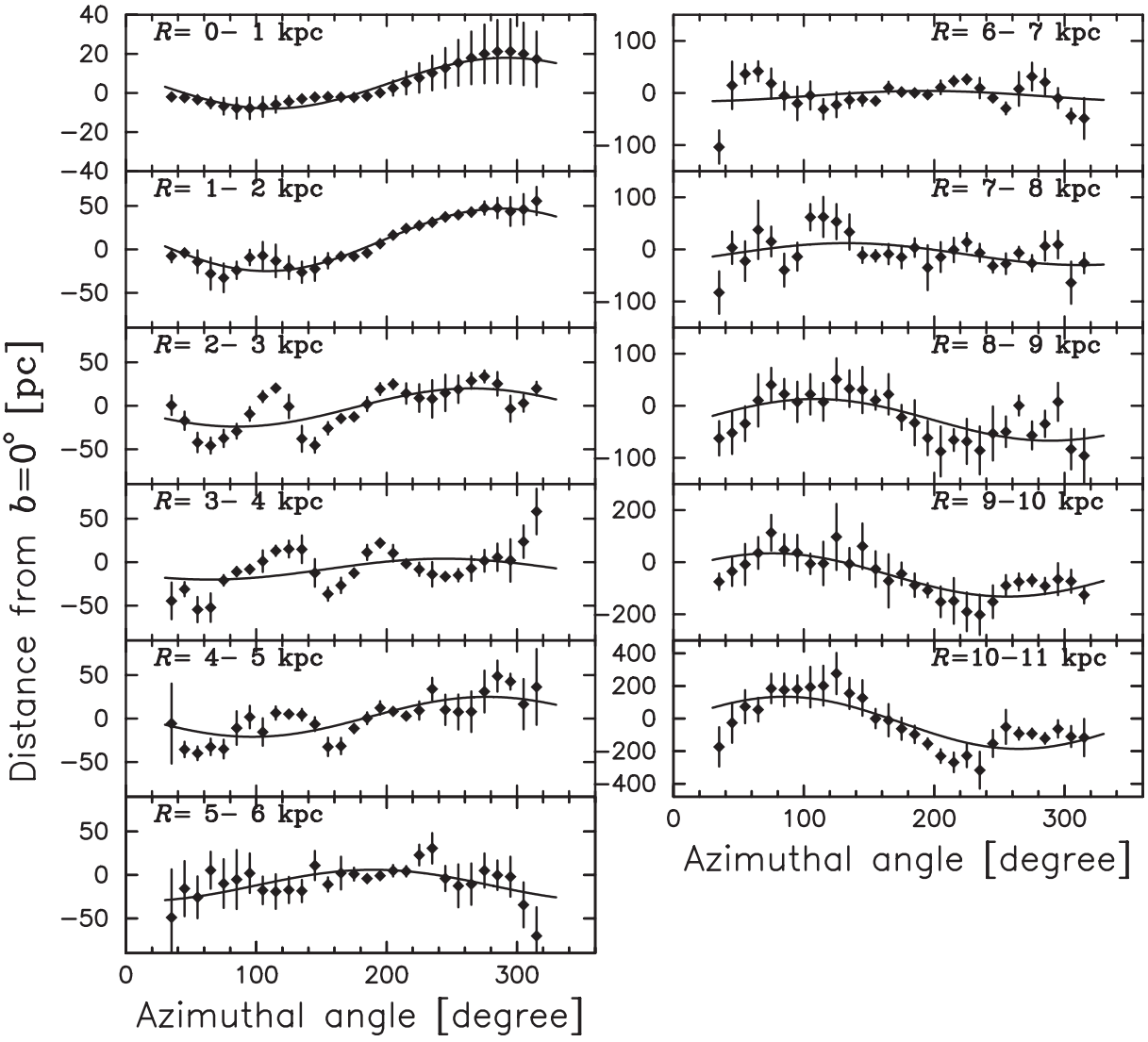

Fig. 11. Midplane displacements for individual radii. The horizontal and vertical axes denote the azimuthal angle around the Galactic center and the distance from the plane of $b = 0°$.

4.2. Vertical Sliced Maps

Figures 7 and 8 present longitudinal sections of the resultant cube sliced with planes that are parallel to the z-axis. We made 6 slices at the azimuthal angles in each figure. The panels of azimuth angles of $\theta = 40°$, $60°$, $80°$, $100°$, $120°$, and $140°$ in figure 8 are in exactly the opposite directions: $\theta = 220°$, $240°$, $260°$, $280°$, $300°$, and $320°$ in figure 7.

5. Structure of the Molecular Disk

5.1. Radial Distribution

Figure 9 shows the radial distribution of the surface density averaged azimuthally over the 1 kpc-width radius when the constant conversion factor was adopted. For comparison, figure 9 also shows radial distributions calculated by Bronfman et al. (1988) and Grabelsky et al. (1987). The radius is reduced by a factor of 8/10 because of a difference in the adopted Galactic constant. Moreover, we adopted a conversion factor of 1.8×10^{20}, although Bronfman et al. (1988) and Grabelsky et al. (1987) used X of 2.8×10^{20}. Hence, we reduced the surface density by a factor of 1.8/2.8. The data from Bronfman et al. (1988) are the mean value of the northern and southern data. The filled squares, open circles, and open triangles denote the data from the present study, Bronfman et al. (1988), and Grabelsky et al. (1987), respectively. The surface density decreases from $26.7\,M_\odot\,\mathrm{pc}^{-2}$ to $0.3\,M_\odot\,\mathrm{pc}^{-2}$ with the Galactocentric distance. Our result is almost consistent with Bronfman et al. (1988) and Grabelsky et al. (1987). The plotted values are given in table 1.

Radial distributions of the molecular gas in spiral galaxies are often expressed with exponential functions (Young et al. 1995). However, this figure shows that the radial profile is not expressed by an exponential function. The surface density is quite high at the Galactic center and near the 4 kpc radius, which is in response to the central condensation and four-kpc

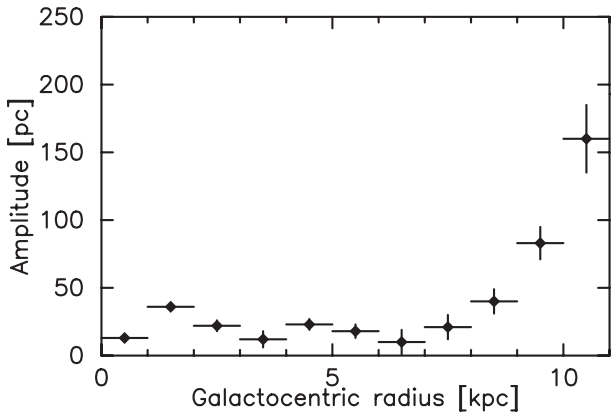

Fig. 12. Amplitude of the midplane displacement versus the Galactocentric distance.

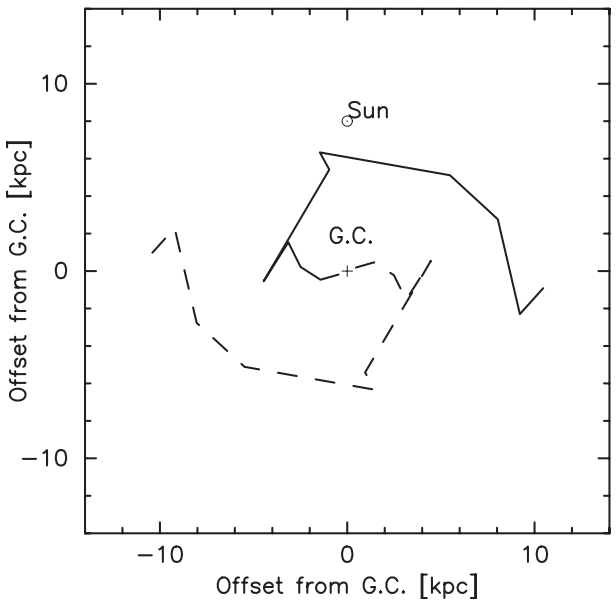

Fig. 13. Loci where the midplane displacements reach the maximum in the face-on view. The solid and dashed lines denote the loci where the midplane is displaced upward and downward, respectively.

ring found in the face-on map. The Galaxy is known to have a bar in the central region (e.g., Nakada et al. 1991). These double peaks are thought to relate to the barred structure (e.g., Nakai 1992).

We also show the radial distribution of the molecular gas density at the midplane in figure 10. Radial distributions derived by Bronfman et al. (1988) and Grabelsky et al. (1987) are plotted for comparison. The radius is reduced by a factor of 8/10, and the density is multiplied by $(1.8/2.8) \times (10/8)^2$ because of the difference in the adopted Galactic constant and the conversion factor. The filled squares, open circles, and open triangles denote the data from the present study, Bronfman et al. (1988), and Grabelsky et al. (1987), respectively. The radial distribution is similar to that of the surface density. The density decreases from $8.73\,\mathrm{cm}^{-3}$ to $0.03\,\mathrm{cm}^{-3}$ with the Galactocentric distance. Our result is almost consistent with Bronfman et al. (1988) and Grabelsky et al. (1987). The radial profile of this value is not expressed by an exponential function, either. The plotted values are given in table 1.

5.2. *Scale-Height*

Figure 3 shows that the FWHM of the molecular gas disk slightly increases from 48 pc to 160 pc with the Galactocentric radius in the radius range of 0–11 kpc. The scale-height is smaller than that of the H I disk. The plotted values are given in table 1.

5.3. *Midplane Displacement*

Figures 7 and 8 show that the midplane of the inner disk is slightly displaced from the Galactic plane, which is known as a midplane displacement, a tilted disk, or a warped disk. The warping of the outer disk was clearly delineated by May, Alvarez, and Bronfman (1997).

Figure 11 shows the midplane displacement versus the azimuthal angle, θ, relative to the Galactic center for individual radii. The vertical axis denotes the distance between the midplane of the molecular disk and the plane of $b = 0°$. We calculated the midplane displacement, z_m, by averaging z with the weight of density, $n(z)$,

$$z_m = \frac{\int z\, n(z)\, dz}{\int n(z)\, dz}. \tag{8}$$

The midplane displacement can be expressed with a sinusoidal function. Hence, the molecular gas disk can be considered as a collection of tilted rings. We fitted the following sinusoidal function to the obtained data:

$$z_m = z_0 + A \sin(\theta - \theta_0). \tag{9}$$

The fitting algorithm used in this paper is the nonlinear least-squares Marquardt–Levenberg algorithm used in a software gnuplot. The obtained parameters are given in table 2. Figure 12 shows that the amplitude of the midplane displacement is nearly constant inside a radius of 10 kpc. However, the

Table 2. Fitted parameters of the midplane.

Radius (kpc)	z_0 (pc)	A (pc)	θ_0 (°)
0–1	5 ± 1	13 ± 1	292 ± 3
1–2	11 ± 1	36 ± 2	288 ± 4
2–3	-2 ± 4	22 ± 4	265 ± 15
3–4	-8 ± 5	12 ± 6	244 ± 32
4–5	2 ± 3	23 ± 4	277 ± 13
5–6	-12 ± 3	18 ± 5	190 ± 13
6–7	-6 ± 6	10 ± 9	193 ± 43
7–8	-9 ± 6	21 ± 9	133 ± 23
8–9	-27 ± 7	40 ± 9	109 ± 15
9–10	-49 ± 10	83 ± 12	76 ± 11
10–11	-26 ± 30	160 ± 25	85 ± 11

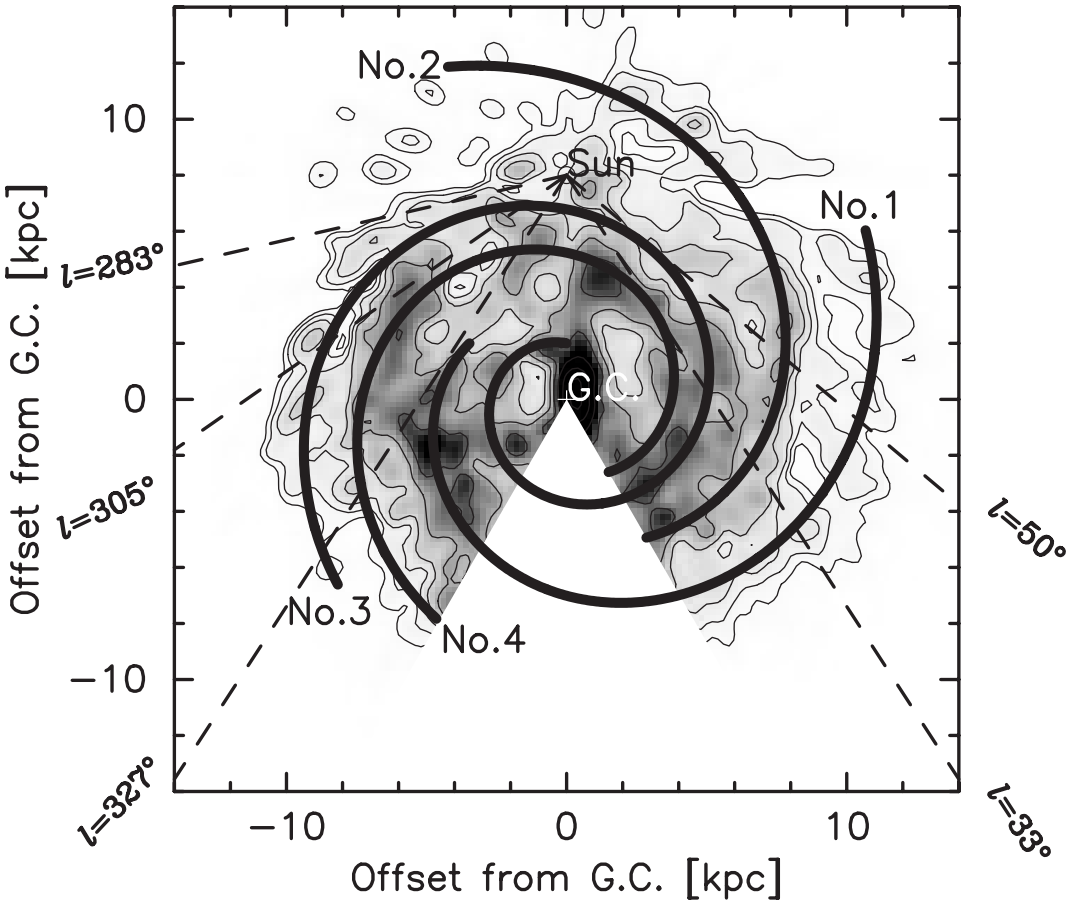

Fig. 14. Schematic tracers of H_2 gas arms superimposed on the obtained H_2 column density map; No.1: Norma–Outer arm; No.2: Perseus arm; No.3: Sagittarius–Carina arm; No.4: Scutum–Crux arm. The contour levels are the same as those of figure 5.

amplitude steeply increases beyond the radius of 10 kpc, where the H I warp is remarkable (Paper I).

Figure 13 shows loci of the maximum points of individual tilted rings. The solid and dashed lines denote the loci where the midplane is displaced upward and downward, respectively. The loci form leading spiral arms, which is consistent with the rules of the warp summarized by Briggs (1990), and is interpreted as follows: The midplane displacement can be considered as a wave, called a bending wave (Binney, Tremaine 1987). Defining Ω and ν as the rotational and vertical frequencies, respectively, the pattern speed of the bending wave is expressed as $\Omega + \nu/m$ or $\Omega - \nu/m$ (m: integer). Since the first one denotes a fast propagating wave and a trailing arm, it disappears rapidly as a result of the winding process. On the other hand, the leading spiral component is long-lived.

5.4. *Central Concentration*

A highly concentrated molecular gas, which is called the central molecular zone (CMZ; Morris, Serabyn 1996), is seen at the Galactic center. The gaseous column density reaches $\gtrsim 25\,M_\odot\,\mathrm{pc}^{-2}$ at the center when we adopt a conversion factor of $1.8 \times 10^{20}\,\mathrm{cm}^{-2}\,\mathrm{K}^{-1}/\mathrm{km\,s}^{-1}$. Though it is plausible that abundant molecular gas is distributed near the Galactic center, the shape shown in this map is suspicious, because the non-circular motion is noticeable in the central region due to the central Galactic bar. Sawada et al. (2004) created a face-on

Table 3. Parameters of schematic spiral arms.

Name	Pitch angle	Beginning point		Ending point	
	(°)	(kpc)	(°)	(kpc)	(°)
Scutum–Crux	12	3.0	30	9.1	330
Sagittarius–Carina	11	2.0	180	10.5	310
Perseus	15	5.7	30	12.6	200
Norma–Outer	15	4.0	240	12.3	120

view of the CMZ using the data from the CO (J = 1–0) survey of the Galactic central region by Bitran et al. (1997). Because they derived it without using the kinematic distance, their map is more reliable. The molecular gas in the CMZ is elongated in the line-of-sight direction. This feature is thought to be associated with a central galactic bar.

5.5. Spiral Arms

5.5.1. Scutum–Crux arm

The positions of the edges of the Scutum–Crux arm in the first and fourth quadrants are $l = 33°$ and $l = 305°$ (Georgelin, Georgelin 1976). In the direction of $l = 305°$, an arm-like structure can be detected around $(R, \theta) \sim (7\,\mathrm{kpc}, 250°)$, which corresponds to a part of the Scutum–Crux. In figure 14, a schematic tracer of the Scutum–Crux arm is presented by a logarithmic spiral arm starting at $(R, \theta) = (3.0\,\mathrm{kpc}, 30°)$ with a pitch angle of 12°. The parameters of these logarithmic spiral arms used in figure 14 are given in table 3.

5.5.2. Sagittarius–Carina arm

The Sagittarius–Carina arm is a famous arm located near the Sun, and is known to arc in the first and fourth quadrants (e.g., Georgelin, Georgelin 1976; Cohen et al. 1985; Dame et al. 1986; Grabelsky et al. 1987, 1988; Clemens et al. 1988; Solomon, Rivolo 1989). According to Georgelin and Georgelin (1976), apparent edges of this arm are $l = 50°$ and $l = 283°$. This arm can be traced by a logarithmic spiral arm with a pitch angle of 11°. In figure 14, a schematic tracer of the Sagittarius–Carina arm is presented by a logarithmic spiral arm starting at $(R, \theta) = (2.0\,\mathrm{kpc}, 180°)$ with a pitch angle of 11°.

5.5.3. Perseus arm

A clear spiral structure can be found to arc from $(R, \theta) \sim (7\,\mathrm{kpc}, 90°)$ to $(R, \theta) \sim (11\,\mathrm{kpc}, 170°)$. This spiral arm is the "Perseus arm". This arm goes by the Sun outside the solar orbit. The shape of this arm in our map is consistent with the result of Clemens, Sanders, and Scoville (1988). A cross section of this arm is found at R = 10–11 kpc in the top panel of figure 7. This arm can be traced more clearly in an (l, v)-diagram of Dame, Hartmann, and Thaddeus (2001), and is detected from $l \sim 55°$ in negative velocity to $l \sim 270°$ in positive velocity.

This arm traced in the molecular gas map is consistent with that detected in the H I map (Paper I). It is more prominent in the H I map. The pitch angle of this arm was estimated to be 15°. In figure 14, a schematic tracer of the Perseus arm is presented by a logarithmic spiral arm starting at $(R, \theta) = (5.7\,\mathrm{kpc}, 30°)$ with a pitch angle of 15°.

5.5.4. Norma–Outer arm

At a larger radius than the Perseus arm, the Outer arm can be traced from $(R, \theta) \sim (9\,\mathrm{kpc}, 50°)$ to $(R, \theta) \sim (11\,\mathrm{kpc}, 120°)$. The Outer arm can also be seen in the longitude–velocity diagram of the CO survey (Dame et al. 2001). This arm appears in the Galactic longitude range of $30 \lesssim l \lesssim 90°$. The Outer arm is also detected in the H I map similarly in the case of to the Perseus arm. This arm traced in the molecular gas map is also consistent with that detected in the H I map, and is more prominent in the H I map. It can be traced with a logarithmic spiral arm with a pitch angle of 15°.

The Outer arm can be found in the vertical sliced map (figure 8). The Outer arm is located at a radius of $R \sim 9$–12 kpc in the $\theta = 80°$, 120°, and 140° panels of figure 8. Particularly in the $\theta = 120°$ and 140° panels, this arm is displaced from the Galactic plane due to warping.

The Norma arm is known to exist in the fourth quadrant (e.g., Georgelin, Georgelin 1976). Georgelin and Georgelin (1976) stated that the apparent edge of this arm is $l = 327°$. In the fourth quadrant of our H_2 gas map, there is an elongated lump with a high H_2 column density in the direction of $l = 327°$, which corresponds to the Norma arm. Though Georgelin and Georgelin (1976) mentioned that the Norma arm is symmetrical to the Sagittarius–Carina arm, the Norma arm seems to be symmetrical to the Scutum–Crux arm, rather than the Sagittarius–Carina arm.

These two spiral arms seem to be the same arm, assuming that the pitch angles of these arms are 15°. Hence, we call these arms the Norma–Outer arm. There are other possibilities of connections of (i) the Norma and Perseus arms and (ii) the Scutum–Crux and Outer arms. However, the radius of the Perseus is expected to be too small to be connected to the Norma arm in the fourth quadrant. Similarly, the radius of the Scutum–Crux arm is too large to be connected to the Outer arm in the first quadrant. Therefore, the connection of the Norma and Outer arms seems to be most natural.

In figure 14, a schematic tracer of the Norma–Outer arm is presented by a logarithmic spiral arm starting at $(R, \theta) = (4.0\,\mathrm{kpc}, 240°)$ with a pitch angle of 15°.

5.5.5. Comparison with arms identified H II region data

In order to evaluate the validity of the spiral arm that we trace, we compare our result with that of Georgelin and Georgelin (1976). We overlay the spiral arms that Georgelin and Georgelin (1976) traced on our tracing spiral arms in figure 15. The sizes of spiral arms are changed so that the distance between the Galactic center and the Sun is the same. The Sagittarius–Carina, the Scutum–Crux, and the Norma arms that we trace are coincident with those traced by Georgelin and Georgelin (1976), although our radii of the Perseus arm in the range $l \gtrsim 90°$ are slightly different from those of Georgelin and Georgelin (1976).

5.6. Ring-Like Structure

In the first quadrant ($0° \leq l \leq 90°$) a ring-like feature is found at $R \sim 4$ kpc, which corresponds to the ring-like structure found by Clemens, Sanders, and Scoville (1988). The difference in the scale of this structure is due to the adopted R_0. Clemens, Sanders, and Scoville (1988) adopted R_0 = 10 kpc, while we adopted R_0 = 8 kpc. Hence, the scale of our map is 4/5 times as large as the map of Clemens, Sanders, and Scoville (1988). We call this structure the four-kpc ring instead of the five-kpc ring, in this paper.

The edge of the four-kpc ring corresponds to l = 30°–40°. This coincides with the edge of the Scutum–Crux arm. In addition, the Sagittarius–Carina arm seems to be merged into the four-kpc ring in the azimuthal range of $\theta \lesssim 120°$. The four-kpc ring may therefore be a complex of two spiral arms and remarkably enhanced as if it was a ring.

Bronfman et al. (1988) pointed out that the radial distribution of molecular gas is flatter in the south hemisphere than in the north, and that the density peak at $0.5\,R_0$ in the north broadens into a plateau in the south. This statement is consistent with

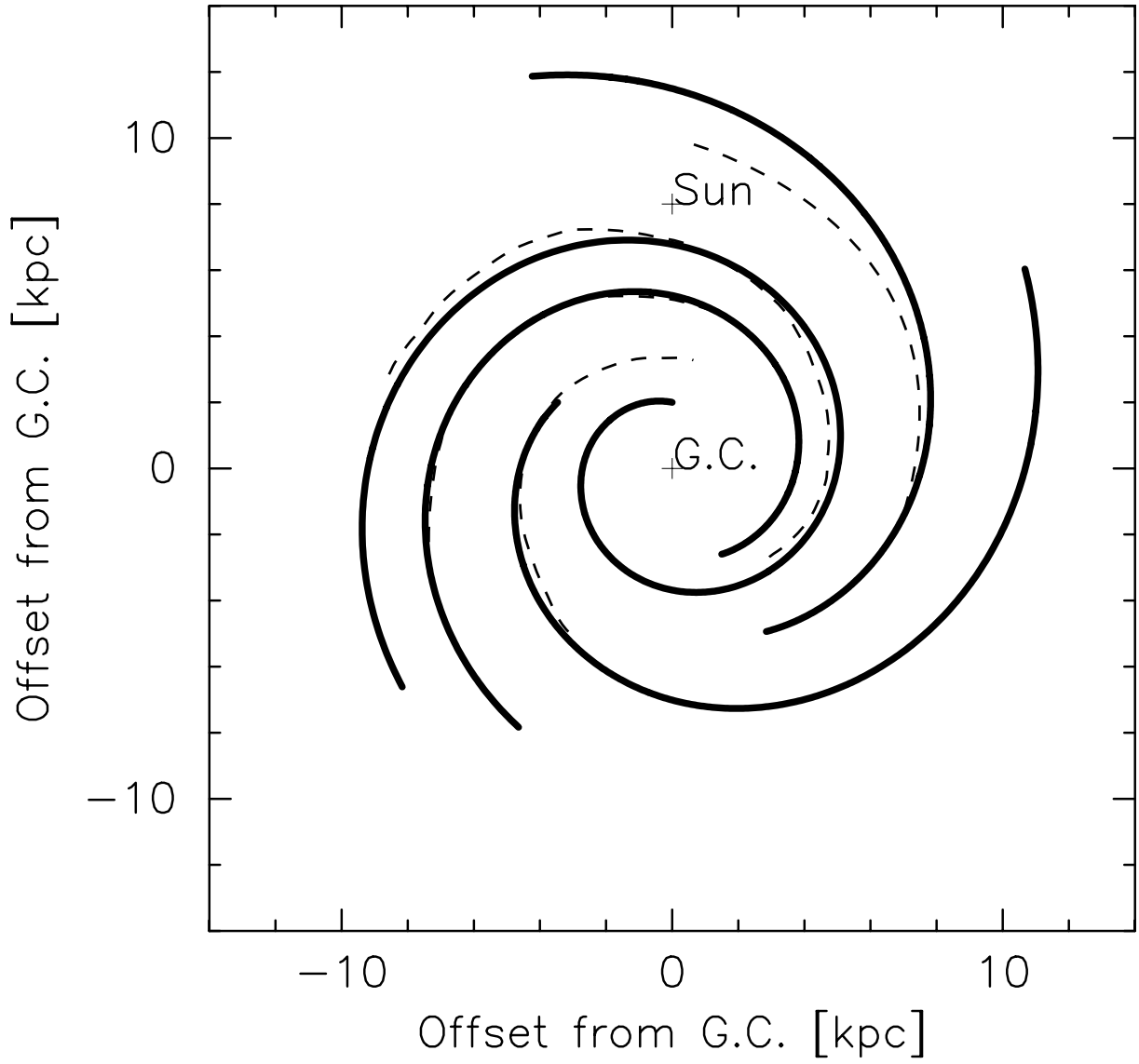

Fig. 15. Comparison of our result and spiral structure presented by Georgelin and Georgelin (1976). The thick lines denote spiral arms that we traced. The thin dashed lines denote spiral arms that Georgelin and Georgelin (1976) traced.

our conclusion that two spiral arms in the south are merged in the north.

6. Possible Errors in Our Molecular Gas Map

Since the molecular gas map we obtained in the present study is based on several assumptions, we must note systematic errors due to deviations from these assumptions.

First, we assumed that the Milky Way galaxy rotates absolutely circularly around the Galactic center. However, the gaseous motion deviates from circular motion due to the density wave or the central Galactic bar, believed to exist at the Galactic center. The isovelocity contours are typically distorted in 1 kpc according to observations of external galaxies. Uncertainties concerning the location of the gas are about 1 kpc.

Second, we used the model expressed by equation (3) to divide the mixture emission from near and far points. Though the resultant map may change due to the adopted function, the global feature is almost the same for any function, as shown in Paper I.

Third, the fitting method does not necessarily work well. The typical residual is less than 20–30% of the midplane density (figure 2). However, the residual becomes much larger near the Sun, which implies that the fitting method does not work well in this region.

Fourth, the conversion factor also affects the resultant gaseous map. We tried to make 3-D maps using a constant conversion factor and a varying conversion factor with the Galactocentric distance. The outer structure was enhanced when we used the varying conversion factor.

7. Summary

We constructed a three-dimensional molecular gas map of the Milky Way galaxy using the new compilation data set of ^{12}CO (J = 1–0) survey obtained with 1.2-m telescopes and the latest rotation curve, based on the kinematic distance. We made molecular gas maps by adopting two types of conversion factors: one is constant, and the other varies with the Galactocentric distance. The two maps are not different in global features.

We present a new 3-D map of the molecular gas in this paper. The resultant maps confirm the following features of the Galactic molecular disk:

1. The radial distribution of the molecular gas surface density has double peaks at the center and at a radius of 0.5 R_0, which is a feature similar to barred spiral galaxies.
2. The FWHM of the molecular disk slightly increases from 48 pc to 160 pc with the Galactocentric distance within a radius range of 0–11 kpc.
3. There is a midplane displacement, whose amplitude is nearly constant inside a radius of 10 kpc, increasing beyond this radius. The ridges of midplane displacement form leading spiral arms.
4. Molecular gas arms corresponding to the Outer, the Perseus, the Sagittarius–Carina, the Scutum–Crux, and the Norma arms could be traced as logarithmic spiral arms with pitch angles of 11°–15°. Supposing that the pitch angles of the spiral arms are within this range, the Norma can be identified as being the same as the Outer arm.

We are grateful to Dr. Thomas Dame et al. for providing us with their large CO survey data. This study was financially supported by a Grand-in-Aid for Scientific Research on Priority Areas (No. 15071202) from MEXT.

References

Alvarez, H., May, J., & Bronfman, L. 1990, ApJ, 348, 495
Arimoto, N., Sofue, Y., & Tsujimoto, T. 1996, PASJ, 48, 275
Binney, J., & Tremaine, S. 1987, Galactic Dynamics (Princeton, NJ: Princeton University Press), subsec. 6.6
Bitran, M., Alvarez, H., Bronfman, L., May, J., & Thaddeus, P. 1997, A&AS, 125, 99
Briggs, F. H. 1990, ApJ, 352, 15
Bronfman, L., Alvarez, H., Cohen, R. S., & Thaddeus, P. 1989, ApJS, 71, 481
Bronfman, L., Cohen, R. S., Alvarez, H., May, J., & Thaddeus, P. 1988, ApJ, 324, 248
Clemens, D. P. 1985, ApJ, 295, 422
Clemens, D. P., Sanders, D. B., & Scoville, N. Z. 1988, ApJ, 327, 139
Cohen, R. S., Dame, T. M., & Thaddeus, P. 1986, ApJS, 60, 695
Cohen, R. S., Grabelsky, D. A., May, J., Alvarez, H., Bronfman, L., & Thaddeus, P. 1985, ApJ, 290, L15
Dame, T. M., et al. 1987, ApJ, 322, 706
Dame, T. M., Elmegreen, B. G., Cohen, R. S., & Thaddeus, P. 1986, ApJ, 305, 892
Dame, T. M., Hartmann, D., & Thaddeus, P. 2001, ApJ, 547, 792
Dehnen, W., & Binney, J. 1998, MNRAS, 294, 429
Georgelin, Y. M., & Georgelin, Y. P. 1976, A&A, 49, 57
Grabelsky, D. A., Cohen, R. S., Bronfman, L., & Thaddeus, P. 1988, ApJ, 331, 181
Grabelsky, D. A., Cohen, R. S., Bronfman, L., Thaddeus, P., & May, J. 1987, ApJ, 315, 122
Hunter, S. D., et al. 1997, ApJ, 481, 205
May, J., Alvarez, H., & Bronfman, L. 1997, A&A, 327, 325
Morris, M., & Serabyn, E. 1996, ARA&A, 34, 645
Myers, P. C., Dame, T. M., Thaddeus, P., Cohen, R. S., Silverberg, R. F., Dwek, E., & Hauser, M. G. 1986, ApJ, 301, 398
Nakada, Y., Onaka, T., Yamamura, I., Deguchi, S., Hashimoto, O., Izumiura, H., & Sekiguchi, K. 1991, Nature, 353, 140
Nakai, N. 1992, PASJ, 44, L27
Nakanishi, H., & Sofue, Y. 2003, PASJ, 55, 191 (Paper I)
Sanders, D. B., Clemens, D. P., Scoville, N. Z., & Solomon, P. M. 1986, ApJS, 60, 1
Sawada, T., Hasegawa, T., Handa, T., & Cohen, R. J. 2004, MNRAS, 349, 1167
Solomon, P. M., & Rivolo, A. R. 1989, ApJ, 339, 919
Solomon, P. M., Rivolo, A. R., Barrett, J., & Yahil, A. 1987, ApJ, 319, 730
Spitzer, L., Jr. 1942, ApJ, 95, 329
Young, J. S., et al. 1995, ApJS, 98, 219